SUPPLEMENT TO THE *WELDING JOURNAL*, MARCH 2013
Sponsored by the American Welding Society and the Welding Research Council

Transient Liquid Phase Diffusion Brazing of Stainless Steel 304

The results of different brazing temperatures and holding times were compared to determine the best condition

BY M. MAZAR ATABAKI, J. NOOR WATI, AND J. IDRIS

ABSTRACT

Transient liquid phase diffusion brazing was employed to join stainless steel 304 using pure copper foil as the interlayer. The brazing process was carried out in a vacuum furnace at various temperatures for a range of times. The joints were studied with optical and scanning electron microscopy, energy-dispersive spectrometry, and corrosion testing. The diffusion of the main elements from the interlayer and base metal into the braze line and brazing-affected areas was the main controlling factor pertaining to the microstractural evolution of the joint interface. The presence of eutectoid γFe+ eutectic Cu + Cr and γFe (Cr, Ni) intermetallic was detected at the interface of the joints brazed with copper interlayer. The average displacement of the solid/liquid interface as a function of time was found to be about 0.36 of the brazing time. The diffusivity of copper in the grain boundary of the stainless steel was found to be around 56×10^5 times higher than the lattice diffusivity at the interface of the joint, showing copper as a melting point depressant has the ability to produce grain boundary grooves facilitating the diffusion of the copper atoms.

Introduction

Austenitic stainless steels have been widely used in nuclear power plants for different applications such as superheaters and heater components, and they are also used in cryogenics and pressure vessels. These steels perform well at elevated temperatures and are applied extensively for steam pipes and exhaust systems. However, there are many difficulties in joining these steels using fusion welding methods. Despite the fact that there is some research on joining stainless steel using gas tungsten arc welding (GTAW), laser beam welding (LBW), and plasma arc welding (PAW), work continues on attaining a reliable joint. A concern, when welding the austenitic stainless steel by conventional welding methods, is the susceptibility to solidification and liquation cracking (Refs. 1–4). In many instances, the formation of brittle intermetallic phases in the diffusion zone leads to unfavorable changes in the mechanical and physical properties of the metallic bonds (Refs. 5–7). The research work presented in this study concerns the transient liquid phase diffusion brazing of stainless steel 304 using a pure copper interlayer. Copper as the interlayer does not form brittle intermetallic compounds with iron, and its melting point is lower than Fe and Ni. Thus, the flowability increases at higher brazing temperatures and encourages a suitable contact between the faying surfaces. The brazing variables and their effect on microstructural changes have been investigated using optical and scanning electron microscopy and energy dispersive spectrometry elemental analyses. In addition, the brazing mechanism was explained using numerical methods. The analysis was coupled with a corrosion test, considering the effects of the brazing parameters.

M. MAZAR ATABAKI (mmazaratabak @smu.edu, mamehdi2@live.utm.my) *is with Research Center for Advanced Manufacturing (RCAM), Department of Mechanical Engineering, Southern Methodist University, Dallas, Tex., and Department of Materials Engineering, Faculty of Mechanical Engineering, Universiti Teknologi Malaysia, Malaysia. J. NOOR WATI and J. IDRIS are with Department of Materials Engineering, Faculty of Mechanical Engineering, Universiti Teknologi Malaysia, Malaysia.*

KEYWORDS

Stainless Steel
Transient Liquid Phase
Diffusion Brazing
Microstructure

Experimental Procedure

The stainless steel was received in the form of plate 2 mm thick, and the chemical composition as shown in Table 1. The plates were cut using an abrasive cutting saw to the dimensions of 2 × 10 × 20 mm. The mating surface of the stainless steel was prepared by conventional grinding on 1200-grade silicon carbide paper followed by polishing using diamond paste. The specimens then were cleaned in an ultrasonic bath using acetone for 15 min and dried in air. A copper foil (50 μm thick, 99.95% purity) was used as intermediate material, and the surface of the interlayer was polished in the same fashion as it does to the base metal. A stainless steel fixture was designed to fix the specimen and hold the sandwich assembly during the metallic brazing process. The brazing process was performed in a vacuum furnace, and the substrate and interlayer contact area was enhanced by a pressure of 0.5 MP at set brazing temperatures. The brazing cycle is shown in Fig. 1. The test specimens were heated to the brazing temperature, then left in the furnace for a variable holding time and heating rate, and finally cooled to room temperature. The brazing parameters for the copper interlayer are shown in Table 2. The specimens were prepared by grinding on 240- to 2400-grade SiC paper, then etched using 2 g $FeCl_3$, 24 mL distilled water, and 6 mL HCl. Microstructural observations were conducted using an optical microscope (Nikon microphot-FXL), scanning electron microscope (SEM, PHILIPS XL 40) using backscattered mode, and energy-dispersive spectrometry (EDS). Moreover, the corrosion test was carried out in a 3.5%

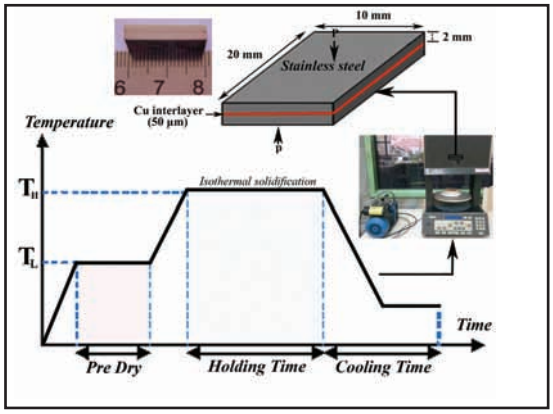

Fig. 1 — Transient liquid phase diffusion brazing cycle and the dimensions of the brazing specimens.

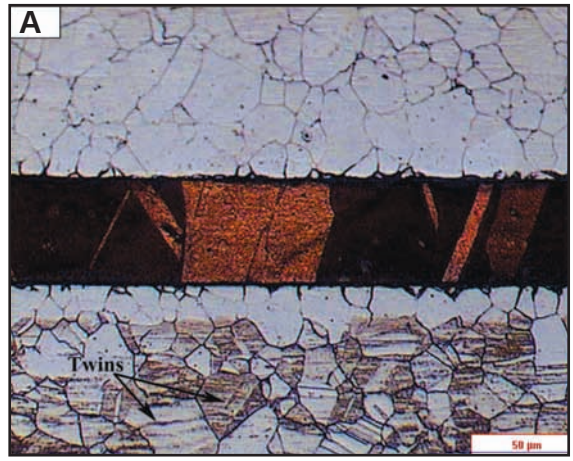

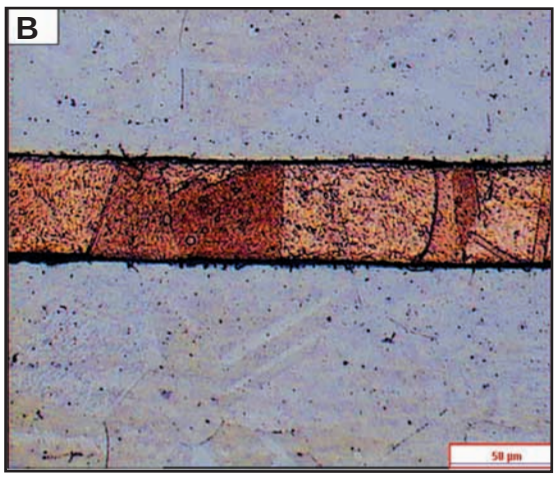

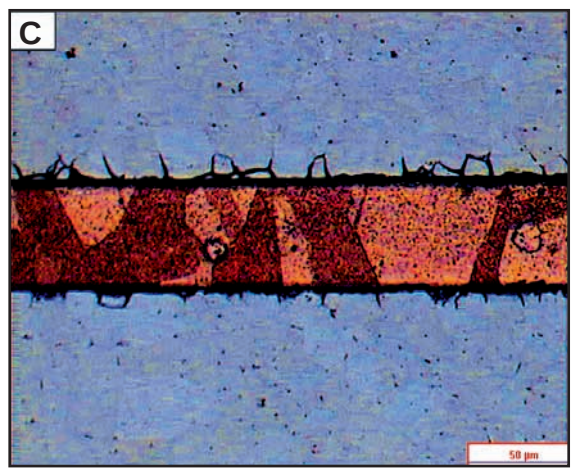

Fig. 2 — The optical microstructure of the joints prepared at A — 900°C; B — 950°C; C — 1000°C for 20 min, using copper interlayer.

NaCl solution in order to determine the corrosion resistance of the bonds. To estimate the reliability of the joints, a shear test was applied using an Instron tensile test machine with a crosshead speed of 1 mm/min.

Results and Discussion

Microstructure Analysis of 304SS-Cu-304SS

Figure 2A–C shows the optical microstructure of the brazed specimens at 900°, 950°, and 1000°C for 20 min holding time, respectively. It is observed that a certain amount of diffusion occurs between the interlayer and two substrates. A thin diffusion layer was revealed parallel to the joint interface on the stainless steel side for all joints. However, it is interesting to note that the stainless steel after exposure to the brazing temperature exhibits different microstructure by emerging twins on the surface of the steel — Fig. 2A. This exposure to the brazing temperature also results in the formation of complex carbides within the austenite grains. This leads to an impoverishment of chromium in the austenite solid solution.

The interface of the stainless steel and copper consisted of a continuous reaction layer free from voids on both sides. It was observed that the copper side showed the absence of any recognizable diffusion zone. Images of the joints prepared at 900°, 950°, and 1000°C for 20 min holding time, shown in Fig. 3A–C, were taken by scanning electron microscope in the backscatter mode. It can be seen that grain boundary grooving increases the diffusion of the main alloying elements due to the curl shape liquid/solid interface and higher grain boundary diffusivity. The effect of the grain boundary grooving was indicated (Refs. 8, 9) considering a significant difference in a predicted brazing time with different grain sizes. Accordingly, if the interfacial curvature enhances the solute, solubility would be increased depending on the stainless steel grain size.

Therefore, increasing the interfacial curvature at the higher temperatures is the reason for enhancing the solute influx into the substrate at both sides of the joint, especially in the diffusion zone. After the grain boundary grooving, the base metal dissolves into the partial molten copper interlayer until the stainless steel in the molten partial melt reaches its equilibrium state at the brazing temperature. While the partial melt touches the stainless steel, a high-carbon iron phase formed and, as a result, the high-carbon iron phase in the molten copper interlayer exceeded its equilibrium quantity. This phase then deposits as a columnar dark structure of Fe-Cu-C phase. This phase grew increasingly with heating time and finally solidified at the interface of the base metal and interlayer.

Therefore, the process of dissolution

Table 1 — Chemical Composition of the Materials (wt-%)

Material	C	Fe	Mn	Si	P	S	Cr	Ni	N	Cu
304 SS	0.08	Bal	2.0	0.75	0.045	0.03	20.0	10.5	0.1	—
Copper Interlayer	—	—	—	—	—	—	—	—	—	99.99

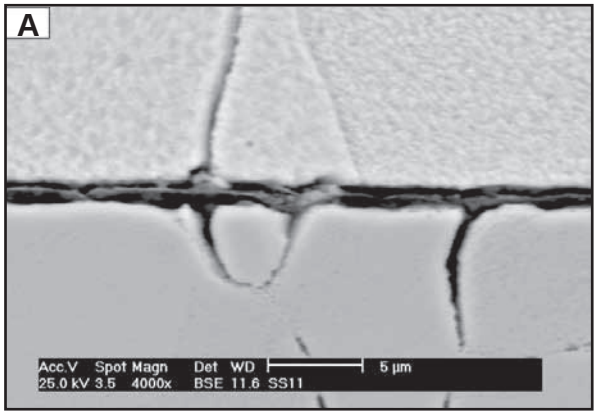

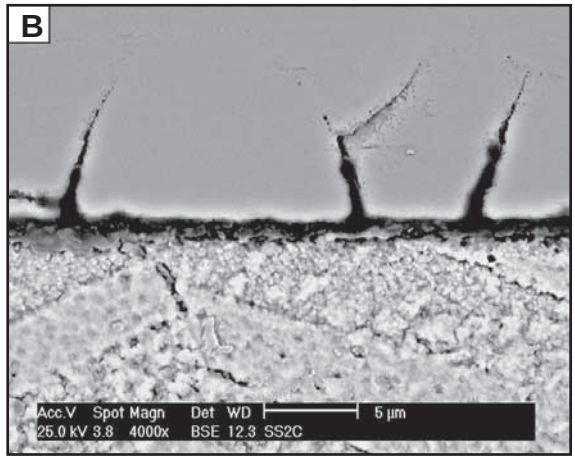

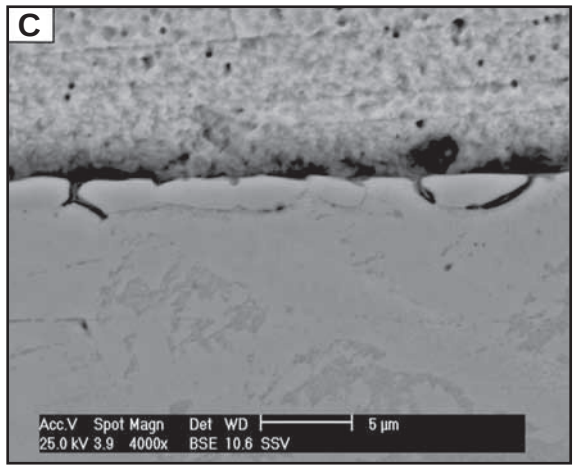

Fig. 3 — SEM-BSE images of the joints prepared at A — 900°C; B — 950°C; C — 1000°C for 20 min holding time.

and solidifying the dark phase can be explained by the distortion of the stainless steel structure due to the diffusion of Cu into the steel. This causes the separation of the formed Fe-Cu solid solution clusters — Fig. 4. In order to determine the chemical composition of the brazing interface, energy-dispersive spectrometry (EDS) analysis was performed using spot analysis taken from the stainless steel and copper interlayer. From the observations, various diffusion zones were found in the joint area and base metal. The brazing-affected zones can be classified in terms of the shape and location of each phase. The area can be divided into three distinct zones, which are base metal, diffusion zone, and interlayer, as shown in Fig. 5. Compositional profiles indicating the distribution of the alloying elements from the base metal and interlayer at the centerline are taken as shown in AB line in Fig. 5. The compositional profile for the specimens brazed at 900°, 950°, and 1000°C are presented in Fig. 6.

Different rates of elemental distribution like the distribution of Fe, Cr, and Cu along the joint is due to the different diffusion coefficients. At the interlayer surface, the side which is rich in Cu, however, only a small amount Fe and Cr diffused from the base metal. It can be seen that the weight-percent of Fe and Cr in the interlayer significantly decreased while the weight-percent of Cu considerably increased in the base metal. The decreasing of Fe at the interface is due to dissolution of the base metal. To further analyze the distribution of Fe and Cr from the base metal to the interlayer and Cu from the interlayer to the base metal, Cu-Fe and Fe-Cr-C phase diagrams were applied for describing the effect of the melting point depressant on the mechanism of the brazing process. A very low amount of Fe was detected in the copper interlayer due to the limited solubility of Fe in copper at the temperature range of 900° to 1000°C. The copper started to dissolve a little amount of Fe at the stainless steel/copper interlayer interface and continuously diffuses into the interlayer.

The diffusion of Cu into the stainless steel produces a solid solution in a very limited solubility. In addition, the solubility of Cu in Fe was enhanced when the brazing temperature was increased. It can be assumed that the diffusion layer at the braze consists of γFe + (Cu). The element distribution analysis revealed that at any of the brazing temperatures, Cu transfered a long distance in the stainless steel side, while Fe, Cr, and Ni transverse a

Table 2 — Bonding Process Parameters

	Brazing Parameters
Low Brazing Temperature (°C)	850, 900, and 950
Predry Time (min)	24
Rate (°C/min)	25
High Brazing Temperature (°C)	900, 950, and 1000
Holding Time (min)	16, 20, 24, and 72
Cooling Time (min)	10
Vacuum (mm Hg)	740
Vacuum Start (mm Hg)	740
Vacuum Release (mm Hg)	740

Table 3 — Average of the Diffusion-Affected Zone Thickness in the Joints Prepared at 900°, 950°, and 1000°C at Various Holding Times

Temperature (°C)	900			950			1000	
Holding Time (min)	16	20	72	16	20	72	20	72
X_1 (µm) – Diffusion Zone	9.286	9.657	15.15	10.013	14.8	16.385	7.581	72
X_2 (µm) – Interlayer	47.129	46.933	46.05	45.113	43.357	43.24	42.355	7.854
X_3 (µm) – Diffusion Zone	7.996	8.664	11.91	6.257	9.748	13.895	5.957	8.432
Predicted $X_{D.Z}$ (µm)	8.245	8.996	13.451	8.452	13.765	14.673	6.941	41.121

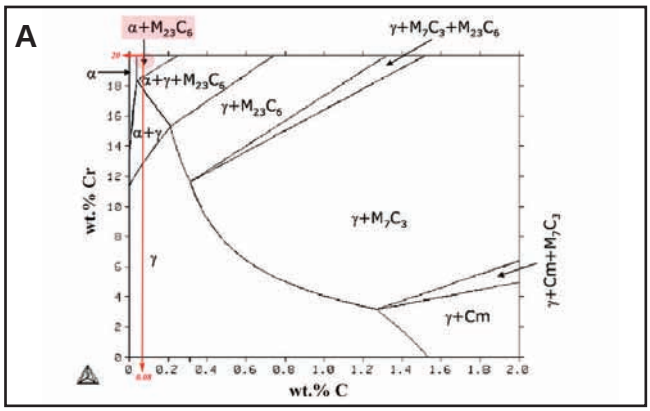

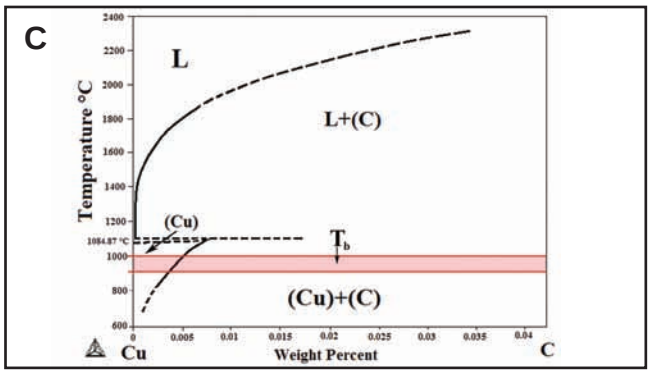

Fig. 4 — Binary alloy phase diagrams. A — Cr-C; B — Fe-Cu; C — Cu-C.

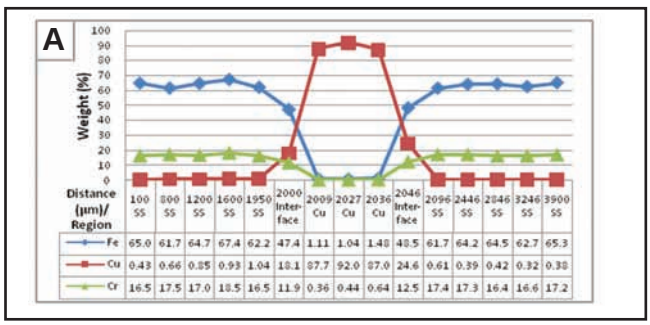

Fig. 6 — Elemental distribution for the joints brazed at A — 900°C; B — 950°C; C — 1000 °C for 20 min holding time.

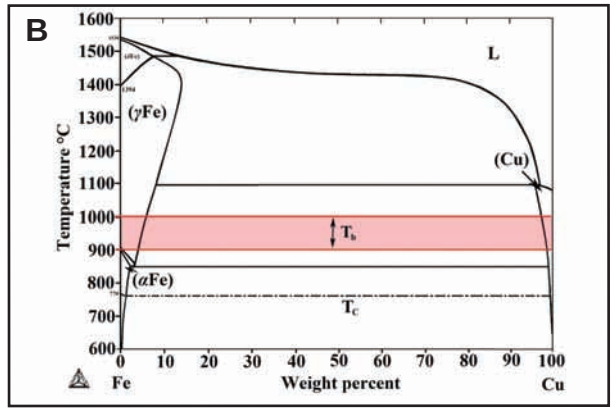

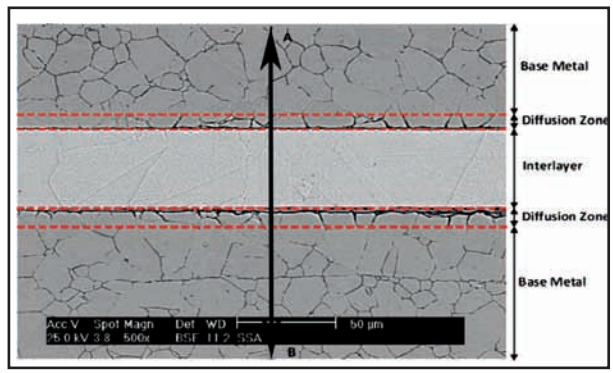

Fig. 5 — Three distinct zones in the joints, showing the solute infiltrated into the grain boundaries of the base metal. This is more obvious in the diffusion zone.

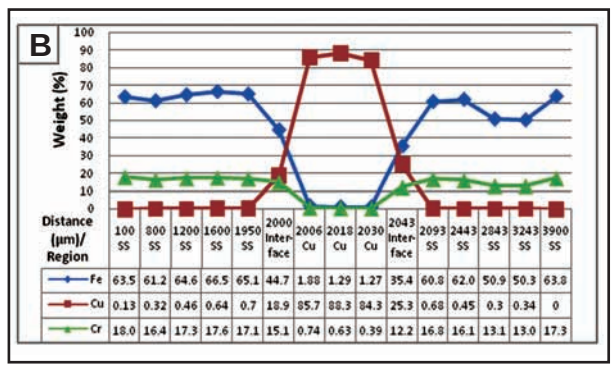

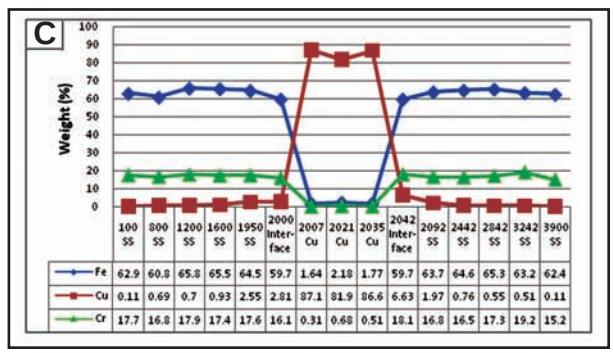

comparatively smaller distance in the Cu interlayer side.

Interface Characterization

For characterizing the diffusion zone and diffusion-affected areas, images were taken from the joint area at the stainless steel/copper interlayer interface as shown in Figs. 8 and 9. Moreover, a quantitative overview of the chemical composition of different regions (region A to E) of the diffusion zone for the specimen brazed at 900°C illustrated in Fig. 7A shows a dark-shaded region (point B) and a light-shaded region (point C) at the interface. By applying EDS analysis, it is shown that regions B and C are enriched with Fe and Cr with small quantities of Ni, Mn, and Cu. The different contrast occurs due to the dissimilarity in concentration of Fe and Cr into the interlayer and Cu into the base metal. The white island (region A) found in the copper interlayer is enriched with Fe and Cr. Figure 7B shows a significant difference in the joint compared to the joints shown in Fig. 7A, presenting a small diffusion layer. Copper is dissolved (regions D and E) due to infiltration of the liquidated copper at 1000°C. Figure 8 shows a schematic diagram describing the possible brazing mechanism and the changes of the phases from the beginning of the process until 20 min of holding time.

At the initial stage, during the brazing process, the copper interlayer partially liquefied and then stainless steel dissolved by migrating the liquid copper to the base metal. As a result, some grain boundary grooves appeared in the steel in the vicinity of the copper interlayer, and Fe-Cr from the base metal flows into the diffusion zone. At the same time, Cu atoms of the melt diffuse into the dissolved region. This is known as a relationship of the solid metal dissolution and liquid metal migration.

While the liquid interlayer touches the surface of the base metal, the migration of

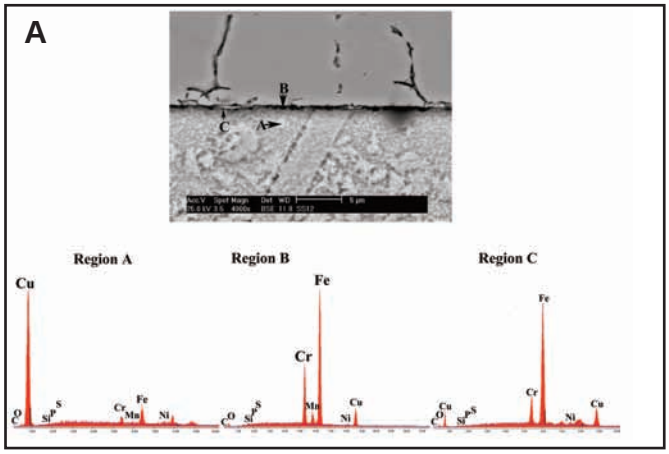

Fig. 7 — A — SEM-BSE image and EDS analysis of the joints prepared at 900°C; B — SEM-BSE image and EDS analysis of the joint prepared at 1000°C.

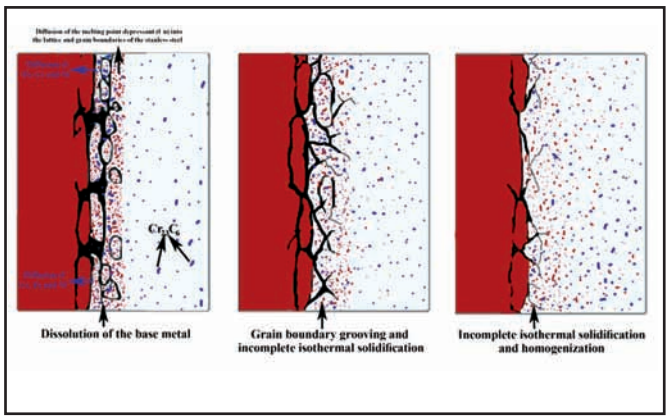

Fig. 8 — Schematic of the brazing mechanism.

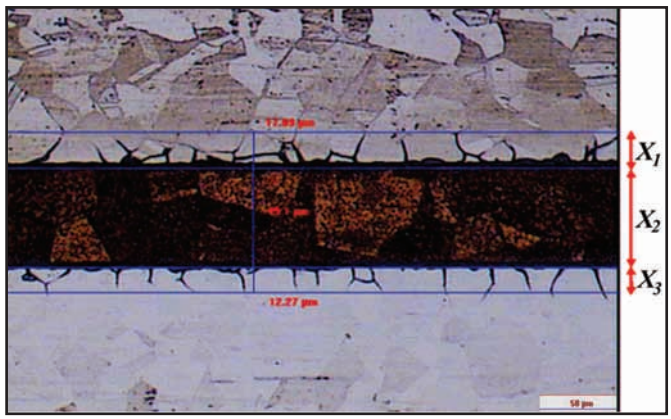

Fig. 9 — The thickness of the diffusion area and its measurement.

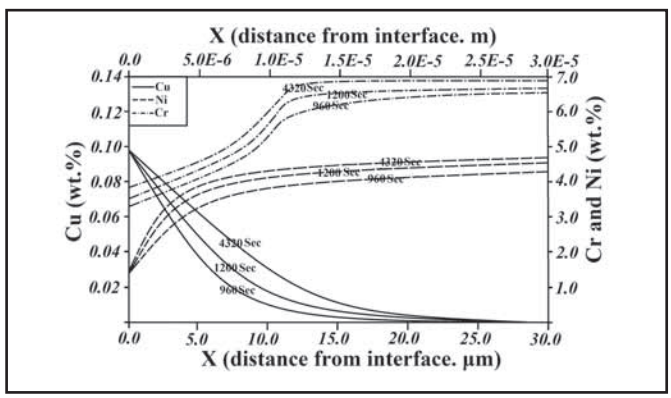

Fig. 10 — The concentration profile of Cu, Cr, and Ni at the interface of the stainless steel and interlayer brazed at 900°C.

the melting point depressant to the base metal occurs by diffusing into the grain boundary of the base metal (Ref. 10). The grain boundary grooving as a result of heavy diffusion of the melting point depressant adjacent to the interfacial region caused great infiltration of copper into the stainless steel. The liquid copper changes into Cu phase and reacts with Fe and Cr along the interface. As described, the diffusion coefficients of Fe, Cr, and Cu are quite different. For example, the diffusion coefficient of Cu into Fe and Fe into Cu at 920°C is 2.2×10^{-13} and 4.63×10^{-10} cm^2/s, respectively (Ref. 11). By increasing the dissolution of the base metal with applying a longer time (16 min), the phase is enriched with Cu and Fe — Fig. 8B.

On the other hand, it was observed that the Fe and Cr atoms that flowed from the base metal were transformed into a Fe-Cr phase. By increasing the holding time to 20 min, the amount of Fe-Cr phase shows a tendency to increase — Fig. 8C.

Widening of Diffusion Zone

The diffusion zone was widened during the brazing operation. The mechanism of the diffusion zone widening is studied by measuring the thickness of the diffusion area on both sides of the interlayer with an initial thickness of 50 µm. The thickness of the diffusion zones for the joint prepared at 950°C for 16 min is shown in Fig. 9. It can be seen that the diffusion zone advanced into the stainless steel. Table 3 shows the average thickness of the diffusion zone for the joints fabricated at 900°, 950°, and 1000°C for various holding times.

As the morphology of the diffusion zone was not uniform, thickness of the diffusion-affected zones was taken at three different locations. It was seen that the thickness of the diffusion zone increased with increased holding time. Generally, mass transfer has to be extended, depending on the brazing temperature. By increasing the brazing temperature more, atoms migrated across the interface, hence the diffusion zone widened. By approaching the melting temperature of the copper interlayer (900°–950°C), Cu atoms were stimulated to move faster and in larger quantity. Therefore, it is enough for Cu atoms to vibrate and give possibility to Fe and Cr atoms to diffuse into the interlayer. If the growth of the diffusion zone assumed to be parabolic, the growth can be stated by a simple relation:

$$X_{D.Z} = \sqrt{D_{Cu \rightarrow Fe} t_b} \qquad (1)$$

where $X_{D.Z}$ is the growth of the diffusion zone, $D_{Cu\ Fe}$ is the diffusion coefficient of Cu atoms into the stainless steel structure, and t_b is the brazing time. Calculating the

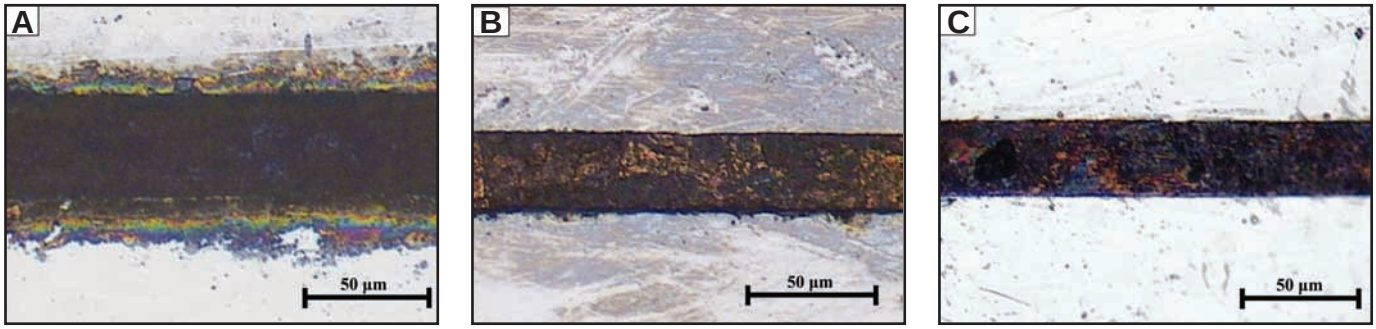

Fig. 11 — The optical microstructure of the joints prepared at A — 900°; B — 950°; C — 1000°C for a holding time of 20 min.

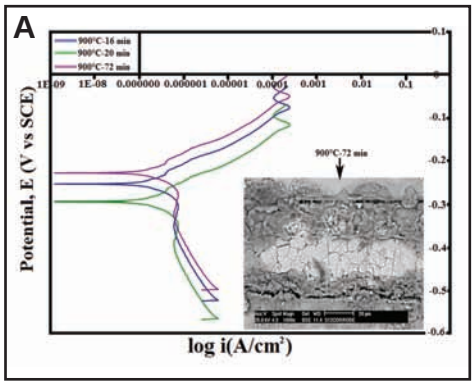

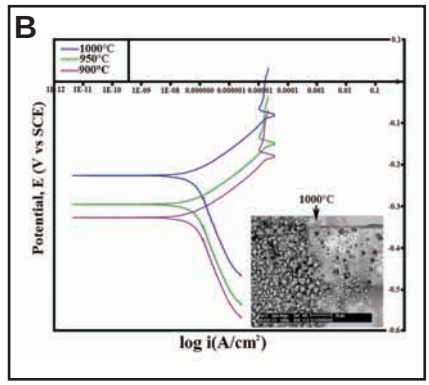

Fig. 12 — A — Linear polarization test results for the joints brazed at 900°C for three different holding times; B — linear polarization test results for the joints prepared at three temperatures for 20 min holding time.

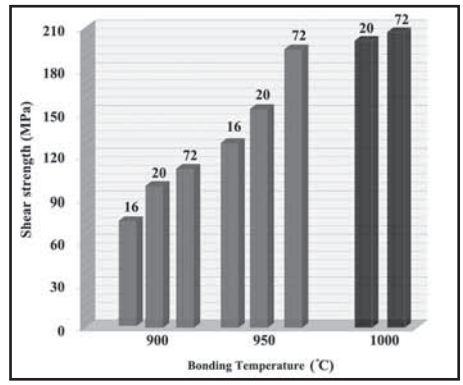

Fig. 13 — The comparison of the shear strengths for the joints prepared at different temperatures and holding times.

growth of the diffusion zone implies that the distance of the movement of Cu atoms into the base metal can be predicted by the simple parabolic law under the condition that other parameters like self-diffusion and Kirkendall effect are neglected from the evaluation (Table 3). To estimate the diffusion coefficient of Cu, Cr, and Ni, the Boltzmann solution of Fick's second law was applied based on the following definition:

$$D_S = \frac{1}{2t_b}\frac{\partial x}{\partial C_S}\int_{C_{S_1}}^{C_S} x\,dC_S \qquad (2)$$

where x is the position of the solute, t_b is the brazing time, and C_S is the concentration of the solute in the stainless steel. It was reported that $D_{Cu\ \rightarrow Fe}$ at 900°C is 4.67×10^{-15} m²/s for a diffusion time of 50 min (Refs. 12, 13), whereas D_{Cu} calculated in this research, despite applying lower diffusion time, is a little higher, reaching to 1.06×10^{-13}. The reason behind this difference might be the presence of Cu in the lattice and grain boundaries of the stainless steel. The predicted value of the Cu diffusion in the grain boundaries of the stainless steel is 1.754×10^{-6}. Another main element in the stainless steel is Ni, which for a stainless steel with 10 wt-% Ni has a predicted diffusion coefficient of 1.5×10^{-14} m²/s at 1280°C with holding specimens at 1280°C (Ref. 14), although the diffusion coefficient of Ni at a brazing temperature of 900°C is estimated to be 2.65×10^{-14} m²/s. The diffusion coefficient of Cr is also predicted to be 5.03×10^{-14} m²/s. Now, with having the diffusion coefficients, the diffusion profiles of Cu, Cr, and Ni in and out of the stainless steel can be estimated by solving the Fick's second law and applying an analytical model:

$$C(t,x)_{Cu,Cr,Ni} = C_0\left(1 - erf\left(\frac{x}{2\sqrt{D_{Cu,Cr,Ni}t_b}}\right)\right) \qquad (3)$$

where $C\ (t, x)_{Cu,Cr,Ni}$ is the composition of each of Cu, Cr, and Ni individually in the joint, D is the diffusion coefficient, t is the brazing time, x is the distance from the interface of the substrate and interlayer, and C_0 is the initial solubility of Cu, Cr, and Ni in the stainless steel. The concentration of Cu, Cr, and Ni can be drawn via distance from the joint as shown in Fig. 10. It can be seen that by increasing the brazing time the concentration of the elements changes considerably leading to a change in the interlayer thickness. However, the thermal activation of the solute atoms was higher at the higher brazing temperatures causing a higher rate of mass transfer and tougher atomic brazing.

Corrosion Test Results

Figure 11A–C shows the optical microstructure of the joints prepared at 900°, 950°, and 1000°C after corrosion test in a 3.5% NaCl solution for 12 h. Dark film deposits were present along the copper surface for all joints. Chloride ions are very aggressive ions to the copper interlayer, due to the tendency of the chloride ion to form unstable films (CuCl and $CuCl_3^{2-}$) (Ref. 16). Therefore, even a little amount of chloride ions can cause severe corrosion attack. Figure 12 shows polarization curves for the joints as a function of the brazing time and temperature. It can be declared that all the joints show the same behavior in the polarization curve due to the uniform and continuous penetration of the solute and other alloying elements. However, optical examination indicated that the corrosion mostly attacks along the surface of the stainless steel and copper interlayer.

Obviously, the cathodic line for the brazing temperature of 900°C exhibits high current density indicating a hydriogenic reaction by reducing the holding time. Thus, the free corrosion potential (E_{corr}) becomes more negative at the lower holding times. Moreover, by reducing the brazing temperature from 1000° to 900°C, cathodic hydrogen reactions are reduced and E_{corr} increases negatively. The anodic polarization curve for all joints shows that the current density significantly

increases as a result of dissolution of the electrode at the beginning of the anodic polarization, and then the current density decreases because of the passivation process. In the passivation region, the joint surface is covered by the passive oxide film. Then, the current density starts to increase suddenly due to the breakdown of the passive layer until the end of the polarization curve.

As mentioned, the corrosion frequently occurred along the stainless steel-copper interface and inside the copper region. At the anodic polarization curve, the current density was significantly increased for all the joints indicating dissolution of some phases (γFe + eutectic Cu + Cr), which resulted in preferential localized corrosion. As indicated in Fig. 12, severe corrosion attack with a wide opening (trench formation) occurred at the interface because of the dissolution of the base metal. The corrosion develops in all the joints and preferential dissolution of the copper interface was favored during polarization. In this case, stainless steel is more positive than copper, so when stainless steel is in contact with copper, the copper corrodes first. The rate of corrosion attack is governed by the size of the potential difference. Referring to the joint, the surface area of the stainless steel is bigger than copper.

As a result, stainless steel has a large surface area in contact with the electrolyte, while the copper interlayer has a very small surface area in contact with 3.5% NaCl solution; therefore, the stainless steel generates a large corrosion current, concentrating on a small area of the copper interlayer. However, intergranular corrosion cracking was found at the copper surface. It is caused by interdiffusion of Fe and Cr along the copper grain boundary and also by Fe-Cr intermetallic compound. The larger the area of the stainless steel, the greater is the acceleration of the copper corrosion.

On the copper side, chloride ions were very aggressive, due to their tendency to form an unstable film (CuCl) and soluble chloride complexes ($CuCl^{2-}$ and $CuCl_3^{2-}$). Besides, intergranular corrosion cracking was also found at the copper surface. It is due to interdiffusion of Fe and Cr elements along the copper grain boundary and also to the formation of Fe-Cr intermetallic phase. This phase dissolves into (Fe + eutectic Cu + Cr) along the interface.

For the joints without an immersion test, there was no pitting attack found on the copper surface, as this can be seen in Fig. 12A. Figure 12B shows a pitting attack on the surface of the copper. Generally, grain boundaries; inclusions such as sulphides, oxides, and nitrides; and local segregation of the alloying elements can act as irregularities, initiating the pitting corrosion. The main alloying elements such as Cr, Ni, and Mo were segregated into the copper interlayer. Pitting corrosion attacks and propagates easily where Cr and Mo contents are locally depleted forming microsegregations, precipitation of carbides, and the formation of intermetallic phases.

A comparison of shear strengths for the joints is shown in Fig. 13. The shear strength increased with the enhancing of brazing time for different temperatures. This increase in joint strength is related to the diffusion of the main alloying elements to the base metal during isothermal solidification, so an optimum brazing time is required to improve the joint strength. The highest shear strength with a value of 180 MPa was achieved for the joints prepared at 950°C for 72 min. It was noticed that the joints prepared at 1000°C showed a reduction in shear strength, confirming the liquation at the grain boundaries of the base metal in the vicinity of the interface.

Conclusions

Transient liquid phase diffusion brazing was applied to join stainless steel using a copper interlayer. Brazing was carried at 900°, 950°, and 1000°C for 16, 20, 24, and 72 min in a vacuum furnace. The important findings are as follows:

1) The microstructure studies revealed that γFe + eutectic Cu + Cr accumulated along the diffusion zone. The diffusion zone for the joints increases with increasing temperature and holding time except for the case of the highest brazing temperature (1000°C), which did not produce significant changes.

2) After brazing, the joint consisted of three distinct zones including base metal, diffusion zone, and diffusion-affected zone. There were no eutectic structures in the joint and a relatively uniform distribution of the alloying elements across the joints occurred, especially at the higher brazing temperature.

3) It was shown that diffusion of Cu in the lattice and grain boundary of the stainless steel plays a significant role in altering the solute concentration in the joint region during the brazing process at the brazing temperatures. Corrosion test results showed that the interface is the weakest part in the resistance against the corrosive solution.

4) The joints developed crevice corrosion due to a galvanic couple formed between the stainless steel and copper interlayer. It presented preferential dissolution of the copper interlayer under anodic polarization in 3.5% NaCl solution at room temperature. Intergranular corrosion was also found in the copper region. After immersing the joints for 12 h, pitting attack appeared at the copper surface. In the shear test, the optimum shear strength was attained for the joints prepared at 950°C for 72 min.

References

1. Orhan, N., Khan, T. I., and Eroglu, M. 2001. Diffusion bounding of a microduplex stainless steel to Ti-6Al-4V. *Scripta Mat.* 45(4): 441–446.

2. Atabaki, M. M., and Hanzaei, A. T. 2010. Partial transient liquid phase diffusion bonding of Zircaloy-4 to stabilized austenitic stainless steel 321. *J. Mat. Character* 61(10): 982–991.

3. Atabaki, M. M. 2010. Microstructural evolution in the partial transient liquid phase diffusion bonding of Zircaloy-4 to stainless steel 321 using active titanium filler metal. *J. Nuc. Mater.* 406(3): 330–344.

4. Atabaki, M. M. 2010. Recent progress in joining of ceramic powder metallurgy products to metals. *Metalurgija-J. Metallurgy* (*MJoM*) 16(4): 255–268.

5. Madaah, H. R. H., Atabaki, M. M., and Tahaei, A. 2003. *Brazing and Soldering,* Jahane Jame Jam Publisher, Tehran, Iran, ISBN 964-95030-5-6, in Persian, p. 127.

6. Atabaki, M. M., and Idris, J. 2012. Low-temperature partial transient liquid phase diffusion bonding of Al/Mg_2Si metal matrix composite to AZ91D using Al-based interlayer. *J. Mater. Des*. 42: 172–183.

7. Mannan, S. K., Seetharaman, V., and Raghuthan, V. S. 1983. A study on interdiffusion between AISI type 316 stainless steel and aluminium. *J. Mater. Sci. Eng.* 60(1): 79–86.

8. Ikeuchi, K., Zhou, Y., Kokawa, H., and North, T. H. 1992. Liquid-solid interface migration at grain boundary regions during transient liquid phase brazing. *Metal. Trans. A* 23A (10): 2905–2915.

9. Ghoneim, A., and Ojo, O. A. 2011. Numerical modeling and simulation of a diffusion-controlled liquid-solid phase change in polycrystalline solids. *Comp. Mater. Sci.* 50(3): 1102–1113.

10. Cramer, S. D., and Covino, B. S. 2003. ASM International, Volume 13A: *Corrosion: Fundamentals, Testing, and Protection*, ISBN: 978-0-87170-705-5.

11. Na, H. S., Kim, J. K., Jeong, B. Y., and Kang, C. Y. 2007. Effect of brazing conditions on microstructure and mechanical properties of duplex stainless steel to Cr-Cu alloy with Cu-base insert metal. *Met. Mater. Int.* 13(13): 511–515.

12. Chang-Gyu, L., Yoshiyaki, I., Tatsuhiko, H., and Ken ichi, H. 1990. Diffusion chromium in α-iron. *Mater. Trans*. 31(4): 255–61.

13. Padron, T., Khan, T. I., and Kabir, M. J. 2004. Modelling the transient liquid phase bonding behaviour of a duplex stainless steel using copper interlayers. *Mater. Sci. Eng. A* 385(1-2): 220–228.

14. Yunker, L. M., and Van Orman, A. J. 2007. Interdiffusion of solid iron and nickel at high pressure. *J. Earth Plan. Sci. Let* 254(1-2): 203–13.

15. E. A. Brandes, G. B. Brook, eds. 1992. *Smithells Metals Reference Book*, 7th ed., Butterworth–Heinemann, Oxford, p. 938.

16. Yeow, C. W., and Hibbert, D. B. 1983. Galvanostatic pulse plating of copper and copper (I) halides from acid copper (II) halide solutions. *J. Electrochem. Soc.* 130(4): 786–90.